Lattice sites of Na dopants in ZnO

U Wahl[1], J G Correia[1], L Amorim[2], S Decoster[2], M R da Silva[3], and L M C Pereira[2]

[1] Centro de Ciências e Tecnologias Nucleares, Instituto Superior Técnico, Universidade de Lisboa, Estrada Nacional 10, 2695-066 Bobadela LRS, Portugal
[2] KU Leuven, Instituut voor Kern- en Stralingsfysica, Celestijnenlaan 200D, 3001 Leuven, Belgium
[3] Centro de Física Nuclear da Universidade de Lisboa, Avenida Professor Gama Pinto 2, 1649-003 Lisboa, Portugal

E-mail: uwahl@ctn.tecnico.ulisboa.pt

Received 29 February 2016, revised 30 May 2016
Accepted for publication 16 June 2016
Published 28 July 2016

Abstract
The angular distribution of β^- particles emitted by the radioactive isotope ^{24}Na was monitored following implantation into ZnO single crystals at fluences above 5×10^{12} cm^{-2} at CERN's ISOLDE facility. We identified sodium on two distinct sites: on substitutional Zn sites and on interstitial sites that are close to the so-called octahedral site. The interstitial Na was to large extent converted to substitutional Na already for annealing at 200°C, from which an activation energy of 0.8−1.3 eV, most likely around 1.2 eV, is estimated for the migration of interstitial Na in ZnO.

Keywords: emission channeling, ZnO, p-type ZnO, sodium, lattice location, diffusion

(Some figures may appear in colour only in the online journal)

CERN-OPEN-2017-002
13/11/2014

1. Introduction

Successful *p*-type doping of ZnO remains one of the challenges that need to be solved before this II-VI wide band gap semiconductor is suitable for wider use in devices [1−3]. Besides doping with group V elements such as N, P, As or Sb, one of the approaches that has been investigated is the use of the group IA alkali metals Li, Na and K or group IB transition metals Cu and Ag, cf the reviews in Refs. [1−4]. These elements should form acceptors if substituting for the group II element Zn. The use of Li and Na to dope ZnO was already investigated in the 1950s, overviews of the early literature on this subject can be found in Refs. [4−7]. With respect to Li, Lander [8] suggested in 1960 that it acts not only as an acceptor (Li_{Zn}^- in its ionized form) but also as interstitial donor Li_i^+, and that its amphoteric nature should complicate its use as efficient *p*-type dopant. Due to the chemical similarity of Li and Na it was assumed that the same holds for Na, although much less experimental studies have investigated this heavier alkali metal. In 1974 an electron paramagnetic resonance (EPR) signal was assigned to substitutional Na_{Zn} on Zn sites [9]. In 2004 EPR and electron nuclear double resonance signals measured in Li and Na doped ZnO nanoparticles were suggested to result from interstitial Li and Na [10−11], although no specific lattice site was proposed. Recently positron annihilation spectroscopy in Na-diffused samples showed a reduction in the concentration of Zn vacancies V_{Zn}, indicating that Na diffusing interstitially had become substitutional by filling up V_{Zn} [12]. The work of Meyer et al [5−7], who studied Li, Na and H-diffused ZnO by means of photoluminescence (PL), suggested that both Li and Na cannot act as shallow acceptors unless found in complexes with H. However, successful *p*-type doping of ZnO by means of Na has been repeatedly reported over the years [13−22].

In contrast to the relatively scarce experimental evidence on the structural aspects of group IA elements in ZnO, a considerable number of theoretical studies have addressed this topic [4,23−32]. While it seems to be a consensus that Li, Na and K are most stable on substitutional Zn sites, several authors proposed that, in particular under O-vacancy rich conditions or when the Fermi level is close to the valence band, they can also occupy interstitial sites. In particular, among the various possible positions in the wurtzite structure (Figure 1), the so-called octahedral sites have been predicted to be the most stable sites for the group IA interstitials [24−28]. From a theoretical point of view it nowadays seems to be accepted that the *p*-type doping efficiency of column-IA elements in ZnO is limited by the formation of compensating interstitial donors.

As mentioned above, so far only indirect experimental evidence has been given on the possible lattice sites of Na in ZnO. In this work, we report on the lattice location of radioactive ^{24}Na implanted into ZnO single crystals determined by means of the β^- emission channeling effect. We give direct

evidence that following low-fluence room temperature (RT) implantation the majority of Na occupies interstitial sites slightly displaced from the ideal octahedral position (I_8) parallel to the c-axis, while following annealing at temperatures at 200°C or above the majority of Na is found on substitutional Zn sites (Na_{Zn}). First experimental estimates for the activation energy of diffusion of interstitial Na and the dissociation of substitutional Na_{Zn} are given as well.

2. Experimental

The radioactive isotope ^{24}Na ($t_{1/2}$ = 14.96 h) was ion implanted into single-crystalline ZnO samples at the ISOLDE on-line isotope separator facility at CERN. At ISOLDE, radioactive Na isotopes are produced by means of 1.4-GeV proton-induced spallation reactions from UC_2 targets. Following out-diffusion of the UC_2 target the Na isotopes are ionized on hot W surfaces, electrostatically accelerated and mass-separated.

Three not intentionally doped ZnO single crystals, all c-axis oriented with a Zn face, were investigated. Samples #1 and #2 (purchased from Eagle-Picher and grown by seeded chemical vapor transport) were implanted with 60 keV ^{24}Na at fluences of 5×10^{12} cm^{-2} and 7×10^{12} cm^{-2}, respectively. Sample #3 (hydrothermally grown and purchased from CrysTec) on the other hand, was simultaneously implanted with 3×10^{13} cm^{-2} of ^{24}Na and 5×10^{14} cm^{-2} of ^{24}Mg at 50 keV. The stable isotope ^{24}Mg, which also originates from the UC_2 target but normally is not present in the ion beam since it is not surface ionized, was added to the ^{24}Na beam by means of element-specific laser-induced Mg ionization [33]. This procedure allowed creating additional damage in the sample while at the same time ^{24}Mg as group II element is not expected to act as an electrical dopant.

For implantation, the samples were mounted on stainless steel sample holders and held in place by stainless steel clamps. All implantations were performed at RT under an angle of 7° to the surface normal in order to avoid channeled implantation and produce well-defined depth profiles. The depth profiles for these implantation conditions, as estimated by means of the MARLOWE code [34], are approximately Gaussian, and for 60 keV energy centered at 663 Å with a straggling of 289 Å and peak concentrations of 1.1×10^5 (atoms/cm^3) / (atoms/cm^2), which for the 5×10^{12} cm^{-2} fluence amounts to 5.5×10^{17} Na atoms/cm^3 or 13 ppm with respect to the Zn concentration. According to MARLOWE, each implanted ^{24}Na atom creates about 260 Zn vacancies.

Thermal annealing was performed *in situ* under vacuum better than 10^{-5} mbar for 10 min for each annealing step. The β^- emission yield in the energy window above 35 keV was measured at RT using the position-sensitive detector systems described in Refs. [35–36] as a function of angle from [0001], [−1102], [−1101], and [−2113] directions in the as-implanted state, as well as after each annealing step.

^{24}Na decays by the emission of β^- particles with an endpoint energy of 1.39 MeV (average β^- energy 556 keV) into the 4.12 MeV excited state of ^{24}Mg, which then de-excites into the ground state of stable ^{24}Mg via a $\gamma\gamma$ cascade, emitting gammas of 2.75 and 1.37 MeV. Emission channeling lattice

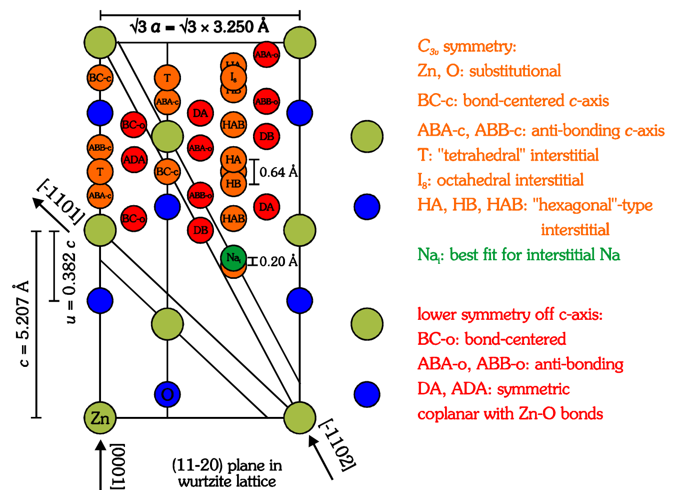

Figure 1. (11−20) plane in the ZnO wurtzite lattice, showing the Zn and O atom positions and the major interstitial sites that were investigated as possible lattice sites of Na. Note that the HA and HB sites are quite close (0.32 Å) to the octahedral interstitial sites I_8 so that the corresponding circles overlap in the picture. Along the [−1102] and [−1101] directions, the double rows of Zn atoms are indicated, the corresponding double rows of O are not marked. The site of interstitial Na_i, which is shifted by (0.23±0.04) Å from the ideal I_8 towards the HA site, is indicated by the green circle.

location experiments with ^{24}Na are challenging since they suffer from considerable background: not only does the isotope possess a quite high β^- endpoint energy but each decay is also accompanied by two high-energy γ particles. Besides background of β^- particles that are backscattered from the sample, sample holder and walls of the vacuum chamber, the position sensitive detector is also exposed to Compton electrons and X rays created in its vicinity by the scattering of γ particles. By means of closing a valve in front of the detector the amount of background resulting from the γ particles was estimated as ~40%. In order to assess the background of scattered electrons we used a Monte Carlo computer code based on the GEANT 4 toolkit [37]. These simulations took into account the composition and geometry of the sample, the sample holder, the detector, and the major parts of the vacuum setup.

Combining both estimates showed that only ~35% of the count rate results from β^- particles directly emitted from the sample towards the detector, with the fraction depending somewhat on the particular experimental setup used. Since the ~65% background events do not contribute to the measured channeling effect, the experimental patterns were corrected for this contribution by subtracting a constant background. This correction introduces an absolute error in the overall sum of fractions of emitter atoms, which is estimated to be around ±(10–15)%, while the relative fractions (e.g. the ratio of substitutional to interstitial sites) are unaffected. Due to this error, the sum of all fractions derived from the analysis may be somewhat larger than 100%. Also, the background of scattered particles depends on the particular experimental setup and since the three samples were measured on three different setups, variations in the sum fractions in between the three

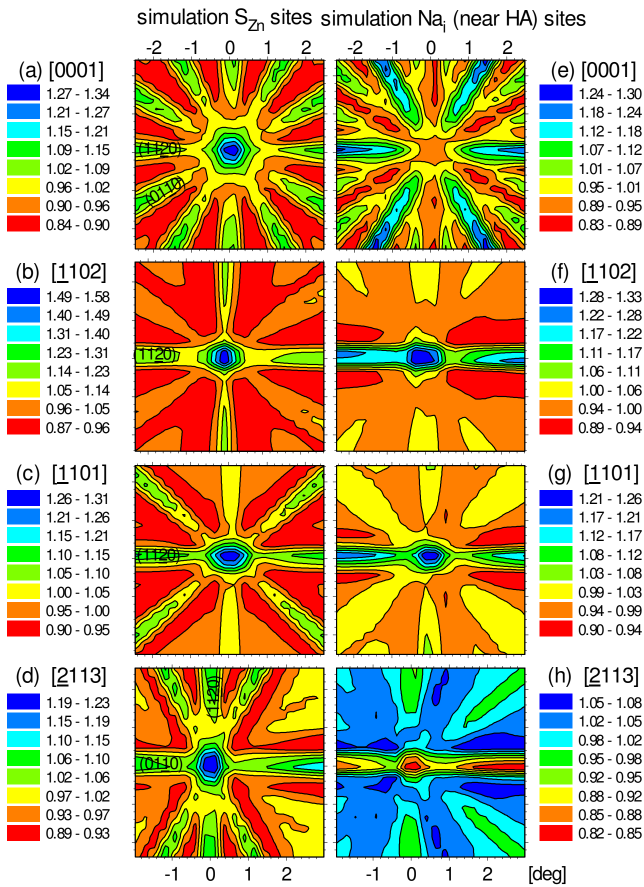

Figure 2. Simulated β^- emission channeling patterns for ^{24}Na in ZnO along the four major crystallographic directions. (a)-(d) are patterns for 100% of emitter atoms on substitutional Zn sites S_{Zn}, while (e)-(h) are for 100% on interstitial sites shifted by 0.2 Å from I_8 towards HA.

samples of the order of ~10% are not considered to be significant.

The evaluation of the probe atom lattice location was performed by quantitatively comparing the experimental patterns with theoretical ones calculated for ^{24}Na on various different lattice sites, using the two-dimensional fit procedure outlined in Refs. [35–36]. The theoretical β^- emission channeling patterns were calculated by means of the "manybeam" theory of electron diffraction in single-crystals [35,38]. Details with respect to the structural properties of ZnO used in the simulations and how to treat continuous β^- spectra have been given previously [39–40]. In the fit procedure, we considered theoretical patterns resulting from emitter atoms at substitutional Zn (S_{Zn}) and substitutional O (S_O) sites, as well as tetrahedral (T), octahedral (I_8) and hexagonal (HA, HB, HAB) interstitial sites with varying isotropic root mean square (rms) Gaussian displacements. A diversity of interstitial sites resulting from displacements parallel or basal to the *c*-axis were also considered. The lattice sites of highest symmetry are illustrated in Figure 1. The "octahedral interstitial" (I_8) positions are sites which are centered exactly between the planes of Zn and O atoms in the wide open space between *c*-axis atomic rows. While in other wurtzite semiconductors, e.g. GaN or AlN,

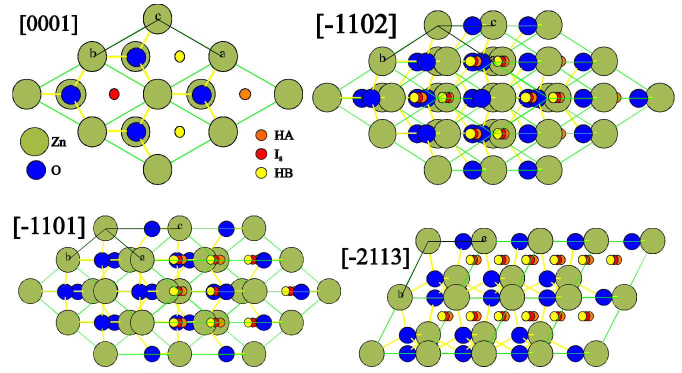

Figure 3. Schematic projections along the major crystallographic directions of a hexagonal ZnO crystal consisting of 8 unit cells. The positions of the interstitial I_8, HA and HB sites are shown as small red, orange, and yellow circles. While the boundaries of the unit cells are shown in green, bonds between Zn and O atoms are indicated in yellow.

these are usually abbreviated as "O" sites, note that we have here used the term "I_8" in order to avoid confusion with the substitutional O sites in ZnO. We have used the designation hexagonal HA or HB sites for interstitial sites that are shifted by +0.32 Å or −0.32 Å from the I_8 sites along the [0001]-axis, both of which are aligned with anti-bonding directions but have Zn or O nearest neighbors, respectively. As HAB sites we designated positions that are a distance of 1.3 Å from I_8 sites, and are also characterized by equal distances towards neighbouring Zn and O atoms.

3. Results

Figure 2 shows the calculated β^- emission channeling patterns for ^{24}Na resulting from 100% of emitter atoms on substitutional Zn sites S_{Zn} and for 100% on sites close to the octahedral interstitial position I_8 (shifted by 0.23 Å towards HA). Since S_{Zn} sites are always aligned with rows and planes of Zn atoms this causes channeling of β^- particles that are emitted under small angles to these directions, and hence an increase in the measured β^- count rate is expected along all axial and planar directions. For interstitial I_8 sites, on the other hand, maxima in β^- count rate are expected along those directions with which the I_8 sites are aligned, and minima along those where they are centered in the interstitial region, cf. Figures 1 and 3. For instance, I_8 sites are perfectly centered within the (11−20) atomic planes, approximately aligned with rows of Zn or O atoms along [−1102] and [−1101] but completely interstitial with respect to the [0001] and [−2113] axes and the (01−10) planes. Correspondingly one expects channeling effects along (11−20), [−1102] and [−1101] but minima along the [0001] axis and the (01−10) planes. The emission patterns for ideal I_8, HA or HB sites differ only slightly from the ones shown.

The angular-dependent β^- emission patterns measured in the RT as-implanted state of sample #1 are shown in Figure 4 (a)−(d) and following annealing at 600°C in Figure 5 (a)−(d). Direct comparison to the theoretical patterns for

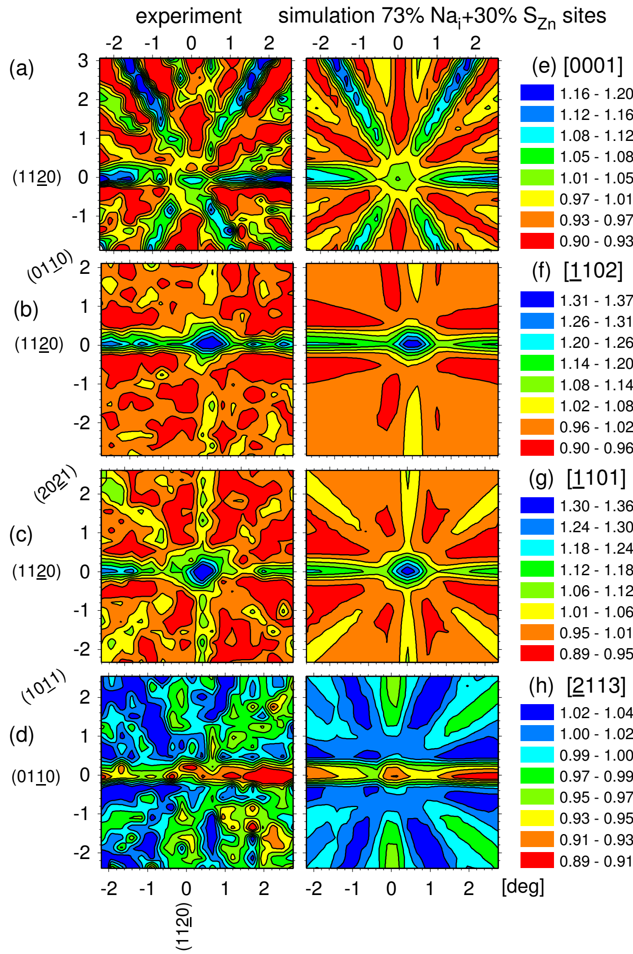

Figure 4. (a)–(d): Normalized β^- emission yield from sample #1 in the vicinity of [0001], [–1102], [–1101], and [–2113] directions in the room temperature as-implanted state. (e)-(h): Best fit results, corresponding to 73% of ^{24}Na on interstitial Na$_i$ as described in the text and 30% on S$_{Zn}$ sites.

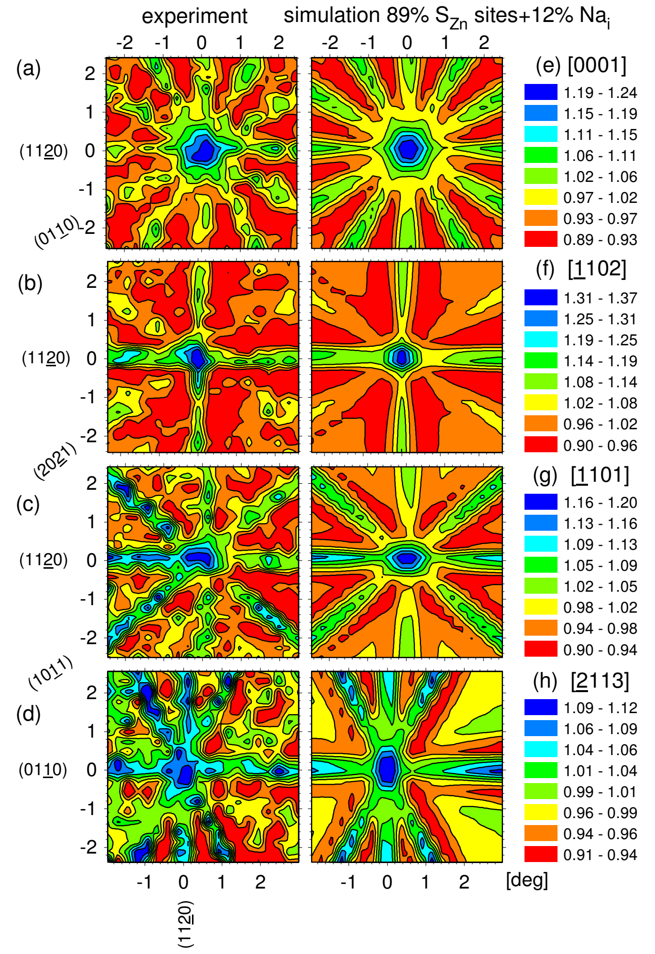

Figure 5. (a)–(d): Normalized β^- emission yield from sample #1 in the vicinity of [0001], [–1102], [–1101], and [–2113] directions following annealing at 600°C. (e)-(h): Best fit results, corresponding to 89% of ^{24}Na on S$_{Zn}$ and 12% on Na$_i$ sites.

I$_8$ sites shown in Figure 2 (e)–(h) indicates that interstitial sites close to I$_8$ account for most of the features observed in the RT as-implanted experimental results. This is most obvious in case of the [0001] and [–2113] patterns. However, there are certain features for which a pure occupancy of I$_8$ sites cannot account, e.g. the small central peak remaining along [0001]. A more detailed quantitative analysis is achieved by means of fitting the experimental yields by a superposition of theoretical patterns for substitutional Zn and interstitial sites plus a constant distribution. In order to test which interstitial position provided the best fit, the location of the interstitial site was varied parallel to the *c*-axis in steps of 0.03–0.05 Å, covering the full range from one HAB to the next HAB position, and including the HA, I$_8$, and HB sites. As is visible from Figure 6, the chi square of fit for all three directions was minimized for a position that is shifted by 0.20–0.29 Å from ideal I$_8$ sites towards the HA position. This site is indicated in Figure 1 as Na$_i$ site. The best fit results for the emission channeling patterns in the RT as-implanted state are shown in Figure 4 (e)–(h) and were obtained for 73% on Na$_i$ sites, 30% on S$_{Zn}$ and a constant angular distribution of –3%. The constant angular distribution accounts for emitter atoms in so-called random sites, which are sites of low crystal symmetry or in heavily damaged surrounding, but also for contributions from the scattering background, as was explained in sect. II. The result that the sum of emitters on HA and S$_{Zn}$ sites is slightly larger than 100% and that correspondingly the constant distribution contributes with a negative value can be attributed to a small overestimation of the background. By performing fits that allowed for three different fractions of emitter atoms on regular lattice sites it was also checked whether other lattice sites could be involved. However, there was no significant improvement in chi square obtained in this case.

In contrast, all major features in the experimental patterns following 600°C annealing [Figure 5 (a)–(d)] are compatible with emitter atoms on substitutional S$_{Zn}$ sites as shown in Figure 2 (a)–(d). As a matter of fact, the detailed fits resulted in fractions of 89% of ^{24}Na on S$_{Zn}$ sites and only 12% on the interstitial positions close to I$_8$ and the corresponding best fit patterns are shown in Figure 5 (e)–(h) and reproduce the experimental results quite well.

In Figure 7 we have displayed the fitted fractions of ^{24}Na on different lattice sites for all three samples as a function of annealing temperature T_A. For sample 1, following the measurements in the RT as-implanted state and following

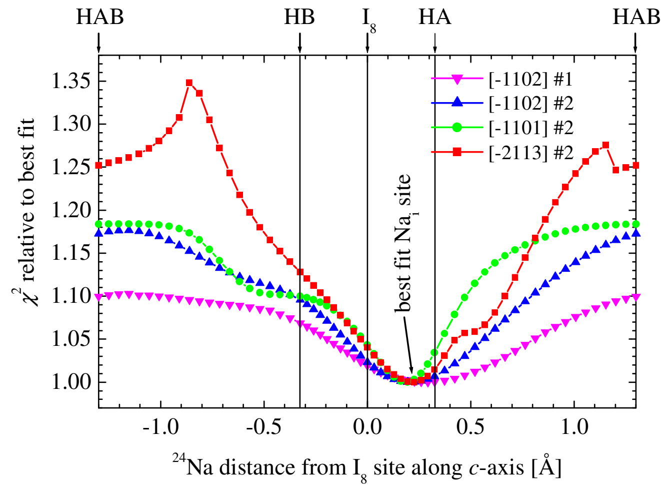

Figure 6. Relative chi square of fit χ^2 as a function of displacement of the major ^{24}Na fraction from the ideal octahedral interstitial site I_8 along the *c*-axis, as derived from the fits of the off-*c*-axis patterns of sample #1 and sample #2 in the RT as-implanted state.

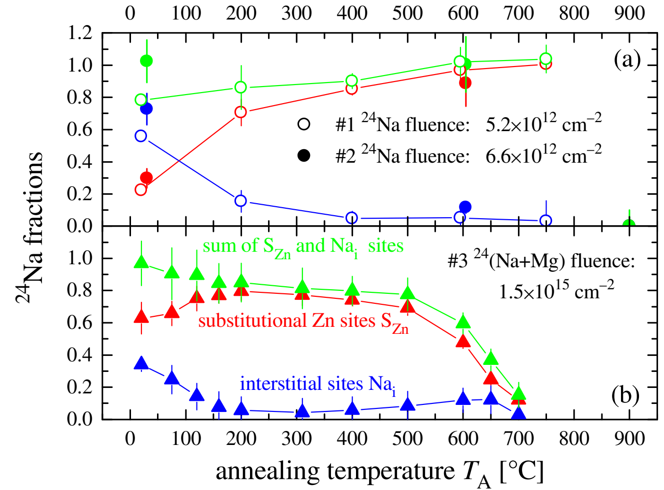

Figure 7. Fitted fractions of ^{24}Na emitter atoms on substitutional Zn (in red) and interstitial Na_i sites (in blue) plus the sum of both (in green) as a function of annealing temperature. Panel (a) shows the results for the low-fluence ^{24}Na-only implanted ZnO samples #1 and #2, while panel (b) are the data for the high-fluence ^{24}Mg co-implanted sample #3.

T_A=600°C, the results of which were described above, an additional annealing step at 900°C resulted in partial outdiffusion of the ^{24}Na from the sample. The β^- emission patterns from the ~50% remaining activity were completely isotropic, consequently we have used a fitted fraction of 0% on any regular lattice sites in Figure 7 (a). For sample #2 annealing steps were performed at 200°C, 400°C, 600°C and 750°C [Figure 7(a)], which showed that already following T_A=200°C a large part of interstitial Na had been converted to substitutional Na on Zn sites. The final anneal of this sample at 750°C resulted in no detectable out-diffusion of Na with 100% remaining on S_{Zn} sites. Finally, sample #3, which was implanted, in addition to 5×10^{14} cm^{-2} stable ^{24}Mg, also with a 4–6 times higher fluence of radioactive ^{24}Na than the other two samples, allowed to perform a larger number of annealing steps [Figure 7 (b)]. Remarkably, in this sample already in the RT as-implanted state 63% of ^{24}Na on S_{Zn} sites was the dominating fraction. The 34% of Na near interstitial I_8 sites was successively converted to substitutional Na as annealing progressed to 200°C, but increased again somewhat up till T_A=650°C. For annealing temperatures at 600°C and above, the S_{Zn} substitutional fraction of Na progressively decreased, with the final 700°C anneal resulting in a 70% drop in count rate from the sample, but leaving ~12% of the remaining ^{24}Na on substitutional Zn sites.

4. Discussion

Our results show unambiguously the existence of interstitial Na in ZnO and its preferred lattice position, which is close to the octahedral interstitial I_8 site, but slightly shifted from the ideal I_8 position towards the HA site. Similar shifts were recently observed for ^{24}Na in GaN and AlN [41]. In the naïve picture of ZnO as an ionic compound formed by Zn^{2+} ions of ionic radius $r(Zn^{2+})$=0.60 Å and $r(O^{2-})$=1.38 Å such a shift would have its explanation in the Na^+ ion being pushed away by the larger O^{2-} ions.

It is interesting to compare our emission channeling lattice location results to β nuclear magnetic resonance (β-NMR) experiments undertaken to measure the nuclear quadrupole moment of the radioactive Na isotopes ^{20}Na and ^{21}Na [42–46]. In these studies spin-polarized Na nuclei were implanted at RT into ZnO single crystals held at a magnetic field of ~0.5 T. The β asymmetry resulting from nuclear decay was then measured as a function of an applied radiofrequency field, resulting in nuclear quadrupole resonance of the nuclei. In all cases it was found that the Na nuclei are exposed to two different electric field gradients (EFGs) in ZnO, roughly at a ratio of 70:30, which was ascribed to two different lattice locations of implanted Na. We note that the ratio of 70:30 between the two fractions of the two different EFGs corresponds almost exactly to the ratio of the fractions of ^{24}Na on interstitial and on substitutional Zn sites (72:33) obtained in our low-fluence emission channeling experiments directly following RT implantation. Since β-NMR experiments are typically performed at implanted fluences which are even lower than in emission channeling experiments, we conclude that the main quadrupole resonance observed in β-NMR of Na in ZnO at RT is due to interstitial Na_i, whereas only the side resonance results from substitutional Na_{Zn}.

Upon annealing to the relatively low temperature of 200°C, interstitial Na_i is converted to large extent to Na_{Zn} on substitutional Zn sites. Our microscopic interpretation of these lattice site changes is that interstitial Na_i starts to migrate between RT and 200°C and then combines with Zn vacancies V_{Zn} that are present in the sample as consequence of the implantation process. This type of site changes from interstitial positions to substitutional cation sites was found for the ion implanted alkali metal Li in a variety of compound semiconductors using alpha emission channeling from the radioactive probe ^{8}Li [47]. The site changes are very effectively promoted by the

fact that the interstitial alkali metals are positively charged ions Li_i^+ and Na_i^+, while the cation vacancies in compound semiconductors usually carry a negative charge Z. This means that when the positive interstitial is within the Coulomb capture radius R_C of the vacancy

$$R_C = \frac{Ze^2}{\kappa k_B T} \qquad (1),$$

where e is the electron charge, k_B the Boltzmann constant, T the temperature and κ the dielectric constant of the semiconductor, thermally activated migration will lead to a drift process of the interstitial towards the vacancy. The activation energy E_M for migration of interstitial Li_i^+ or Na_i^+ can then be estimated using a drift model [47] by

$$E_M = k_B T_{1/2} \ln\left[\frac{3Ze^2 D_0 \Delta t_{ann}}{\kappa k_B T_{1/2}\langle r_i^3\rangle}\right] \qquad (2),$$

where $T_{1/2}$ is the temperature at which half of the interstitial probes have been converted to substitutional (≈145°C = 418 K for ^{24}Na in ZnO sample #2), Δt_{ann} = 10 min is the annealing time, and D_0 the entropy constant of the interstitial migration. For ZnO the negative charge of the cation vacancy should be $Z = -2$ [4,48–49]), so that using $\kappa = 8.5$ one arrives at R_C = 94 Å. On the other hand, from MARLOWE simulations [33] for 60 keV ^{24}Na implantation in ZnO one obtains $\langle r_i^3\rangle^{1/3}$ = 6.6 Å as root mean cube distance, which means that Na_i^+ would be well within the Coulomb capture radius of the nearest vacancy V_{Zn}^{2-} resulting from its own implantation process, so that the application of this correlated capture drift model makes sense. The entropy constant D_0 of the interstitial migration of Na_i can be estimated as follows:

$$D_0 = \frac{r_M^2 \nu_0}{6} N_{NN} \qquad (3),$$

where ν_0 is the attempt frequency, r_M the jump distance, and N_{NN} the number of accessible nearest neighbour jump sites. In principle r_M and N_{NN} may depend in ZnO on whether diffusion occurs only along the c-axis (N_{NN} = 2, r_M = 2.60 Å), only perpendicular to it (N_{NN} = 6, r_M = 3.25 Å), or both (N_{NN} = 8, $r_M \approx$ 3.09 Å), however, since D_0 appears as argument in the logarithm, this distinction is here of minor importance. Using a typical $\nu_0 = 10^{12}$ s^{-1} of the order of the lattice vibrations, the estimated value for the migration energy of interstitial Na_i in ZnO using the correlated capture drift model is thus E_M = 1.25−1.32 eV.

A somewhat different approach to estimating E_M is by means of N-step jump models, where one assumes that the interstitial Na has to make a certain number of jumps N until it is being captured by V_{Zn}. In such models the fraction $f_i(T)$ of Na which remains on interstitial sites following annealing at temperature T is given by

$$f_i(T) = f_{i0} \exp\left[-\frac{\nu_0 \Delta t_{ann}}{N} \exp\left(-\frac{E_M}{k_B T}\right)\right] \qquad (4),$$

where f_{i0} is the interstitial fraction before the anneal and all other variables are as defined above. Solving for E_M, one arrives at

$$E_M = k_B T \ln\left[\frac{\nu_0 \Delta t_{ann}}{N \ln(f_{i0}/f_i)}\right]. \qquad (5).$$

The models then require reasonable assumptions about the number of steps. First, one can assume as lower limit of jumps that N = 1, i.e. the implanted Na_i is located directly neighbouring to V_{Zn}. This results in $E_M(N{=}1)$ = 1.24 eV for sample #2, a value that is close to the one derived from the drift approximation. This is understandable since in the drift approximation we used the assumption that the root mean cube distance of Na_i to the next V_{Zn} is $\langle r_i^3\rangle^{1/3}$ = 6.6 Å, as obtained from MARLOWE simulations, requiring only a very small number of jumps. However, since dynamic annealing of vacancies occurs already during the implantation and afterwards, the number of vacancies will be significantly reduced, so that also an upper limit for N should be considered. For that purpose a reasonable assumption is that the diffusion-induced broadening of the implantation profile $(r_M^2 N/3)^{1/2}$ is less than the mean implantation depth of ^{24}Na (663 Å), which would require N to be smaller than ≈138000, resulting in E_M > 0.81 eV.

We will now focus on what can be learned from the results of sample #3, to which the high-fluence co-implantation of ^{24}Mg was applied. Obviously, in this sample the initial interstitial fraction of ^{24}Na is much smaller than in the low-fluence implanted samples, making substitutional Na_{Zn} already the dominating lattice site following RT implantation. First let us consider the order of magnitude that the temperature of the sample as a whole may have been raised during the implantation. While the energy deposited by the fluence of 5.3×10^{15} cm^{-2} of 50 keV ^{24}Mg+^{24}Na into a beam spot of 1 mm diameter corresponds to 1.4×10^{17} eV, this amounts to only 0.20 meV per atom in the 5×5×0.5 mm^3 sample as a whole, which is quite negligible compared to the RT thermal energy of ~25 meV. If it were limited to the 1 mm diameter area of the sample hit by the beam, the energy introduced corresponds to 6.3 meV/atom which without further dissipation would lead to a temperature increase of ~20 K (specific heat of ZnO is 41.1 J/mol/K). Since the implantation lasted 15 min much of this energy will be distributed over a larger area of the sample. At the microscopic level the energy introduced by each implanted ion results in a damage cascade that cools down after a thermal spike. During high-fluence implantations these thermal spikes may overlap in space and time which may raise the effective temperature in the implanted region, however, to quantitatively assess this effect is beyond the scope of this work. From the ^{24}Mg+^{24}Na fluence of 5.3×10^{14} cm^{-2} and the number of ~260 Zn vacancies created per implanted ion one estimates a peak Zn vacancy concentration of 1×10^{22} cm^{-3}. This means that in the peak of the implantation profile every 5−6th Zn atom has been displaced. The fact that the ZnO sample essentially still retains its single crystal structure is a consequence of the very efficient dynamic annealing processes that take place in this material and that are responsible for its well-known exceptional radiation hardness [50–51].

We should also briefly discuss the likely influence of changes in the electrical characteristics of the ZnO samples caused by the implantation. Not intentionally doped ZnO single crystals are generally n-type, i.e. the Fermi level should be close to the conduction band. When damage was introduced

by MeV oxygen or medium energy (0.1−1 MeV) transition metals, it was observed that undoped ZnO in the as-implanted state gradually became isolating, i.e. *n*-type carriers were removed [51−52] and the Fermi level should move towards mid gap. On the contrary, the implantation of Si [53], Al [54], C [55] or Ge [56] strongly decreased ZnO resistivity by means of inducing additional *n*-type carriers, also already in the as-implanted state. However, in these latter cases it was not clear to what extent the *n*-type carriers were induced by possible electrical donor activity of radiation damage or the implanted impurity. In ^{57}Mn Mössbauer experiments it was observed that the implantation of 1.4×10^{13} cm^{-2} of ^{23}Na at 60 keV was able to change the predominant ionization state of Fe in ZnO from Fe^{2+} to Fe^{3+}, which was explained by radiation damage induced changes of the Fermi level towards mid gap [57]. This would mean that in our case already the low-fluence ^{24}Na implantations in samples #1 and #2 (5×10^{12} cm^{-2} and 7×10^{12} cm^{-2}) may have been accompanied by a shift of the Fermi level, an effect that would be even more pronounced in the high-fluence Mg-implanted sample #3. A further shift of the Fermi level towards mid gap, however, should favour the inclusion of Na on interstitial sites [23−26] in comparison to sample #1 and #2, which was not observed. Therefore, the increased substitutional fraction of Na in sample #3 directly following implantation is most likely to be explained by a combination of excess thermal energy and Zn vacancies. Moreover, the Zn vacancy concentration was probably so high that the application of a 1-step model best describes the lattice site changes of Na upon annealing. Using this approach, one obtains a value of $E_M = 1.17$ eV for the migration energy of interstitial Na. Summarizing, the migration energy E_M of interstitial Na_i in ZnO as estimated from site changes of ^{24}Na observed by emission channeling and using the drift approximation or reasonable *N*-step models is in the range 0.81−1.32 eV, however, we consider a value around 1.2 eV quite likely. Huang et al [27] have theoretically predicted the migration energy Na_i to be 0.74 eV perpendicular to the *c*-axis and 1.33 eV parallel to it. Our estimates hence coincide well with this energy range.

We also tried to give an estimate for the activation energy of dissociation E_A of Na from substitutional Zn sites. If this process leads to subsequent long-range diffusion or to Na being trapped in highly-defective regions of the sample, it shows up in the emission channeling site fractions as changes from substitutional to random sites, and, after replacing E_M by E_A and f_i by the substitutional fraction f_s, eq. (5) can be used to derive E_A. However, in this case our results currently do not allow to reach a clear conclusion. In the ^{24}Mg high-fluence co-implanted sample #3 already annealing at 600°C and above lead to progressive decrease of the substitutional ^{24}Na fraction. Neuvonen et al [58−59] observed that the shape of the profile of 150 keV high fluence (10^{15} cm^{-2}) implanted Na in ZnO changed after 30 min annealing at 550–600°C, while for the lower Na fluence of 10^{14} cm^{-2} an annealing temperature of 800°C was needed in order to cause a similar effect. In our studies, the substitutional fraction in the low-fluence implanted sample #2 stayed constant up to the highest annealing temperature used in this case (750°C), and only in sample #1 partial out-diffusion of Na for $T_A = 900$°C clearly proved long-range migration. It thus looks as if the stability of Na on substitutional sites is lower in samples that have suffered more severe radiation damage, which is poorly understood and would require further studies. We tentatively estimate the activation energy for dissociation of substitutional Na E_A to be in the range 2.0–3.3 eV. Huang et al in their work [27] only have calculated values for the activation energy for dissociation of substitutional Li_{Zn} in the two different charge states −1 and 0, $E_A(Li_{Zn}^{-1}) = 3.41$ eV, $E_A(Li_{Zn}^{0}) = 3.24$ eV, stating that "Na_{Zn}, K_{Zn} and Ag_{Zn} are much more stable than Li_{Zn}".

Lattice location experiments with ^{24}Na have been previously performed also in hexagonal GaN and AlN [41,60], that in many aspects have quite similar properties to ZnO. It is hence not surprising that also in these two III-nitride semiconductors co-existence of ^{24}Na on interstitial sites near the octahedral position and on substitutional cation Ga or Al sites was found, although the maximum interstitial fractions in the RT as-implanted state were with 40-60% lower than in ZnO. The most striking difference, however, was the stability of interstitial Na against thermal annealing. With the conversion of interstitial to substitutional Na in GaN and AlN only clearly visible around 900°C, the migration energies estimated were $E_M(Na_i) = 2.2$–3.4 eV in GaN and $E_M(Na_i) = 2.0$–2.6 eV in AlN [41], meaning that interstitial Na diffuses considerably faster in ZnO than in those two nitrides.

5. Conclusions

In addition to confirming that Na dopants prefer Zn sites in ZnO, our results have given first direct evidence of the existence of interstitial Na_i. We have shown that Na_i prefers the vicinity of the octahedral interstitial sites I_8 rather than the tetrahedral interstitial T sites, in agreement with the predictions in several theoretical papers [24–28]. However, Na is slightly shifted by 0.23 Å from the ideal I_8 site parallel to the *c*-axis towards the HA position, i.e. located somewhat closer to the nearest Zn atoms and further away from O atoms. The amount of interstitial Na is reduced when additional radiation damage is created in the sample, which we ascribe to the increase in the number of available Zn vacancies. The interstitial Na is to large extent converted to substitutional Na already for annealing at 200°C, from which an activation energy of 0.8–1.3 eV, most likely around 1.2 eV, is estimated for the migration of interstitial Na_i in ZnO. Greater uncertainty exists regarding the activation energy for dissociation of substitutional Na E_A, which we tentatively estimate to be in the range 2.0–3.3 eV.

Acknowledgments

This work is dedicated to the memory of our colleague Peter Weilhammer from CERN, who led the development of the position-sensitive Si pad detectors used in this and numerous other emission channeling studies and who passed away on May 27, 2016. We acknowledge the beam time provided by

the ISOLDE collaboration. This work was funded by the *Portuguese Foundation for Science and Technology* (FCT), through project CERN/FIS-NUC/0004/2015 and strategic project UID/Multi/04349/2013. The ISOLDE beam times were supported by the *European Commission* through the 7th Framework program (project number 262010 ENSAR).

References

[1] McCluskey M D and Jokela S J 2009 Defects in ZnO *J. Appl. Phys.* **106** 071101

[2] Ye Z, He H, Lu J and Zhu L 2012, *p*-type ZnO: Current status and perspectives, chapter 4 in *Handbook of Zinc Oxide and Related Materials* vol 1, ed Z C Feng, Taylor and Francis

[3] Fan J C, Sreekanth K M, Xie Z, Chang S L and Rao K V 2013 *p*-Type ZnO materials: Theory, growth, properties and devices *Progress in Materials Science* **58** 874

[4] Janotti A and Van de Walle C G 2009 Fundamentals of zinc oxide as a semiconductor *Rep. Prog. Phys.* **72** 126501

[5] Meyer B K, Alves H, Hofmann D M, Kriegseis W, Forster D, Bertram F, Christen J, Hofmann A, Straßburg M, Dworzak M, Haboeck U and Rodina A V 2004 Bound exciton and donor-acceptor pair recombinations in ZnO *phys. stat. sol.* (b) **241** 231

[6] Meyer B K , Zeuner A and Sann J 2005 Lithium and sodium acceptors in ZnO *Superlattices and Microstructures* **38** 344

[7] Meyer B K, Stehr J, Hofstaetter A, Volbers N, Zeuner A and Sann J 2007 On the role of group I elements in ZnO *Appl. Phys.* A **88** 119

[8] Lander J J 1960 Reaction of Li as a donor and acceptor in ZnO *J. Phys. Chem. Solids* **15** 324

[9] Zwingel D and Gärtner F 1974 Paramagnetic and optical properties of Na-doped ZnO single crystals *Solid State Comm.* **14** 45

[10] Orlinskii S B , Schmidt J, Baranov P G, Hofmann D M, de Mello Donega C and Meijerink A 2004 Probing the wave function of shallow Li and Na donors in ZnO nanoparticles *Phys. Rev. Lett.* **92** 047603

[11] Baranov P G, Orlinskii S B, de Mello Donega C and Schmidt J 2010 High-frequency EPR and ENDOR spectroscopy on semiconductor quantum dots *Appl. Magn. Reson.* **39** 151

[12] Parmar N S and Lynn K G 2015 Sodium doping in ZnO crystals *Appl. Phys. Lett.* **106** 022101

[13] Yang L L, Ye Z Z, Zhu L P, Zeng Y J, Lu Y F and Zhao B H 2007 Fabrication of *p*-type ZnO thin films via DC reactive magnetron sputtering by using Na as the dopant source *J. Electronic Mater* **36** 498

[14] Lin S S, Ye Z Z, Lu J G, He H P, Chen L X, Gu X Q, Huang J Y, Zhu L P and Zhao B H 2008 Na doping concentration tuned conductivity of ZnO films via pulsed laser deposition and electroluminescence from ZnO homojunction on silicon substrate *J. Phys.* D*: Appl. Phys.* **41** 155114

[15] Lin S S, Lu J G, Ye Z Z, He H P, Gu X Q, Chen L X, Huang J H and Zhao B H 2008 *p*-type behavior in Na-doped ZnO films and ZnO homojunction light-emitting diodes *Solid State Comm.* **148** 25

[16] Lin S S, He H P, Lu Y F and Ye Z Z 2009 Mechanism of Na-doped *p*-type ZnO films: Suppressing Na interstitials by codoping with H and Na of appropriate concentrations *J. Appl. Phys.* **106** 093508

[17] He H, Lin S, Yuan G, Zhang L, Zhang W, Luo L, Cao Y, Ye Z and Lee S T 2011 Single-crystalline sodium-doped *p*-type ZnO and ZnMgO nanowires via combination of thin-film and nano techniques *J. Phys. Chem. C* **115** 19018

[18] Lai J J, Lin Y J, Chen Y H, Chang H C, Liu C J, Zou Y Y, Shih Y T and Wang M C 2001 Effects of Na content on the luminescence behavior, conduction type, and crystal structure of Na-doped ZnO films *J. Appl. Phys.* **110** 013704

[19] Liu H, Pan X, Ding P, Ye Z, He H and Huang J 2012 Effects of diffusion temperature and diffusion time on fabrication of Na-diffused *p*-type ZnO thin films *Materials Letters* **80** 175

[20] Lin S S 2012 Robust low resistivity *p*-type ZnO:Na films after ultraviolet illumination: The elimination of grain boundaries *Appl. Phys. Lett.* **101** 122109

[21] Ding P, Pan X H, Ye Z Z, Huang J Y, Zhang H H, Chen W and Zhu C Y 2013 Realization of *p*-type nonpolar *a*-plane ZnO films via doping of Na acceptors *Sol. State Comm.* **156** 8

[22] Wang Z, Liu H, He H, Huang J, Chen L and Ye Z 2015 Determination of Na acceptor level in Na^+ ion-implanted ZnO single crystal *Appl. Phys.* A **118** 1229

[23] Park C H, Zhang S B and Wei S H 2002 Origin of *p*-type doping difficulty in ZnO: The impurity perspective *Phys. Rev.* B **66** 073202

[24] Lee E C and Chang K J 2004 Possible *p*-type doping with group-I elements in ZnO *Phys. Rev.* B **70** 115210

[25] Wardle M G, Goss J P and Briddon P R 2005 Theory of Li in ZnO: A limitation for Li-based *p*-type doping *Phys. Rev.* B **71** 155205

[26] Lee E C and Chang K J 2006 *p*-type doping with group-I elements and hydrogenation effect in ZnO *Physica* B **376** 707

[27] Hu J and Pan B C 2008 Electronic structures of defects in ZnO: Hybrid density functional studies *J. Chem. Phys.* **129** 154706

[28] Huang G Y, Wang C Y and Wang J T 2009 First-principles study of diffusion of Li, Na, K and Ag in ZnO *J. Phys.: Condens. Matter* **21** 345802

[29] Carvalho A, Alkauskas A, Pasquarello A, Tagantsev A K and Setter N 2009 A hybrid density functional study of lithium in ZnO: Stability, ionization levels, and diffusion *Phys. Rev.* B **80** 195205

[30] Du M H and Zhang S B 2009 Impurity-bound small polarons in ZnO: Hybrid density functional calculations *Phys. Rev.* B **80** 115217

[31] Yang X P, Lu J G, Zhang H H, Lu B, Huang J Y, Ye C L and Ye Z Z 2012 Unexpected positive role of oxygen vacancies in Na-doped ZnO *J. Appl. Phys.* **112** 113510

[32] Lyons J L, Janotti A and Van de Walle C G 2014 Effects of hole localization on limiting *p*-type conductivity in oxide and nitride semiconductors *J. Appl. Phys.* **115** 012014

[33] Catherall R, Fedosseev V N, Köster U, Lettry J, Suberlucq G, Marsh B A and Tengborn E 2004 Recent developments in production of radioactive ion beams with the selective laser ion source at the on-line isotope separator ISOLDE *Rev. Sci. Instr.* **75** 1614

[34] Robinson M T 1989 Slowing-down time of energetic atoms in solids *Phys. Rev.* B **40** 10717

[35] U. Wahl 2000 Advances in electron emission channeling measurements in semiconductors *Hyperf. Inter.* **129** 349

[36] Wahl U, Correia J G, Czermak A, Jahn S G, Jalocha P, Marques J G, Rudge A, Schopper F, Soares J C, Vantomme A and Weilhammer P 2004 Position-sensitive Si pad detectors for electron emission channeling experiments *Nucl. Instrum. Meth. Phys. Res.* A **524** 245

[37] Agostinelli S et al 2003 GEANT4 - a simulation toolkit *Nucl. Instrum. Meth. Phys. Res*. A **506** 250

[38] Hofsäss H and Lindner G 1991 Emission channeling and blocking *Physics Reports* **201** 121

[39] Wahl U, Rita E, Correia J G, Alves E and Araújo J P 2003 Implantation site of rare earths in single-crystalline ZnO *Appl. Phys. Lett.* **82** 1173

[40] Wahl U, Correia J G, Mendonça T and Decoster S 2009 Direct evidence for Sb as a Zn site impurity in ZnO *Appl. Phys. Lett.* **94** 261901

[41] Amorim L M 2016 Lattice site location of electrical dopant impurities in group-III nitrides, PhD thesis, KU Leuven, Belgium.

[42] Ogura M et al 2004 Quadrupole Moments of Na Isotopes *Hyperf. Inter.* **159** 235

[43] Minamisono K et al 2004 Quadrupole moments of $^{20,21}Na^*$ *Nucl. Phys.* A **746** 501c

[44] Minamisono K et al 2009 Quadrupole moments of neutron-deficient 20,21Na *Phys. Lett.* B **672** 120

[45] Minamisono K et al 2010 Nuclear polarization of short-lived Na isotopes maintained in single crystals for β-NMR spectroscopy *Nucl. Instr. Meth. Phys. Res.* A **616** 45

[46] Minamisono K et al 2011 Low-energy test of second-class current in beta decays of spin-aligned F-20 and Na-20 *Phys. Rev.* C **84** 055501

[47] Wahl U 1997 Emission channeling studies of Li in semiconductors *Physics Reports* **280** 145

[48] Janotti A and Van de Walle C G 2006 New insights into the role of native point defects in ZnO *J. Cryst. Growth* **287** 58

[49] Janotti A and C.G. Van de Walle 2007 Native point defects in ZnO *Phys. Rev.* B **76** 165202

[50] Kucheyev S O, Williams J S, Jagadish C, Zou J, Evans C, Nelson A J and Hamza A V 2003 Ion-beam-produced structural defects in ZnO *Phys. Rev.* B **67** 094115

[51] Kucheyev S O, Jagadish C, Williams J S, Deenapanray P N K, Yano M, Koike K, Sasa S, Inoue M and Ogata K 2003 Implant isolation of ZnO *J. Appl. Phys.* **93** 2972

[52] Zubiaga A, Tuomisto F, Coleman VA, Tan H H, Jagadish C, Koike K, Sasa S, Inoue M and Yano M 2008 Mechanisms of electrical isolation in O^+-irradiated ZnO *Phys. Rev* B **78** 035125

[53] Izawa Y, Matsumoto K, Kuriyama K and Kushida K 2010 Evaluation of zinc interstitial in Si-ion implanted ZnO bulk single crystals by a Rutherford backscattering study: An origin of low resistivity *Nucl. Instrum. Meth. Phys. Res.* B **268** 2104

[54] Oga T, Izawa Y, Kuriyama K, Kushida K and Kinomura A 2011 Origins of low resistivity in Al ion-implanted ZnO bulk single crystals *J. Appl. Phys.* **109** 123702

[55] Izawa Y, Matsumoto K, Oga T, Kuriyama K, Kushida K and Kinomura A 2011 Evaluation of carbon interstitial in C-ion implanted ZnO bulk single crystals by a nuclear reaction analysis study: An origin of low resistivity *AIP Conf. Proc.* **1399** 69

[56] Kamioka K, Oga T, Izawa Y, Kuriyama K and Kushida K 2013 Origins of Low Resistivity and Ge Donor Level in Ge Ion-implanted ZnO Bulk Single Crystals *AIP Conf. Proc.* **1566** 79

[57] Mantovan R et al 2012 Fe charge state adjustment in ZnO upon ion implantation *J. Phys.: Condens. Matter* **24** 485801

[58] Neuvonen P T, Vines L, Kuznetsov A Y, Svensson B G, Du X, Tuomisto F and Hallén A 2009 Interaction between Na and Li in ZnO *Appl. Phys. Lett.* **95** 242111

[59] Neuvonen P T, Vines L, Venkatachalapathy V, Zubiaga A, Tuomisto F, Hallén A, Svensson B G, and Kuznetsov A Y 2011 Defect evolution and impurity migration in Na-implanted ZnO *Phys. Rev.* B **84** 205202

[60] Ronning C, Dalmer M, Uhrmacher M, Restle M, Vetter U, Ziegeler L, Hofsäss H, Gehrke T, Järrendahl K and Davis R F 2000 Ion implanted dopants in GaN and AlN: Lattice sites, annealing behavior, and defect recovery *J. Appl. Phys.* **87** 2149